A 32-Channel C-Band Hybrid Wavelength/ Polarization Division (de)multiplexer on Silicon

Hang Yu, Yuxiang Yin, Xingrui Huang, Donghe Tu, Zhiguo Yu, Huan Guan, and Zhiyong Li

***Abstract*—A 32-channel hybrid (de)multiplexer on silicon is designed and experimentally demonstrated to enable polarization division multiplexing (PDM) and wavelength division multiplexing (WDM) for improving the capacity of optical communication links. The hybrid (de)multiplexer is realized by monolithically integrating a polarization rotator and splitter (PRS) and two 16-channel microring resonators (MRRs) arrays. The through and cross ports of the PRS are connected to the bus waveguide of the MRR arrays, respectively. In order to ensure a larger free spectrum range (FSR) to cover all wavelength channels, the radius of the microring is about 3 μm and the wavelength-channel spacing is 1.6 nm. For the hybrid (de)multiplexer, the crosstalk between the adjacent channels and the non-adjacent channels are −20 dB and −25 dB, respectively. When TE_0 mode input, the insertion loss is 1.5 dB–3.8 dB, the crosstalk between the through and cross port is less than −24 dB. When TM_0 mode inputs, the insertion loss is 1.9 dB–4.5 dB and the polarization crosstalk is less than −22 dB. In order to eliminate the influence of the fabrication errors and temperature on resonance wavelength, a TiN thermal tuning electrode is added to calibrate the deviation of the wavelength.**

***Index Terms*—Polarization-division-multiplexer, wavelength-division-multiplexer, microring, polarization rotator and splitter, silicon.**

I. Introduction

IN RECENT years, the photonic integrated circuit (PIC) with ultra-high capacity are desired to satisfy the demands for a massive increase in data transmission [1], [2]. Several multiplexing/demultiplexing technologies are utilized to improve the capacity of communication links, such as wavelength division multiplexing (WDM), mode division multiplexing (MDM), and polarization division multiplexing (PDM). Among them, WDM is one of the most mature technologies, which has been widely applied to optical communication systems by utilizing multiple wavelength channels [3], [4], [5], [6]. However, due to the limitation of the bandwidth of the erbium-doped fiber amplifier, the available wavelength band is finite. The emergence of PDM and MDM provides new dimensions for multiplexing technology [7], [8], [9]. Therefore, it's viable to combine multi-wavelengths, multi-modes, and dual polarizations to realize a hybrid multiplexing technology. In this way, the data transmission capacity can be further increased to satisfy the demand of the high-speed data transmission for optical interconnect systems as well as decrease the cost of the communication.

In order to realize the on-chip high-performance hybrid (de)multiplexer, silicon photonics integration has been regarded as one of the most attractive implements [10], [11], [12]. For example, in [13], a silicon-based 64-channel hybrid WDM-MDM (de)multiplexer was demonstrated by combining a 4-mode-channel (de)multiplexer based on asymmetric directional couplers (ADCs) and a 16-wavelength-channel arrayed-waveguide-grating (AWG) (de)multiplexer with a channel spacing of $\Delta\lambda_{ch}$ = 3.2 nm, the crosstalk of adjacent wavelength channel is about −14 dB. In [14], an 18-channel hybrid (de)multiplexer was demonstrated by integrating a 9-wavelength-channel bi-directional AWG with a polarization diversity circuit. The wavelength-channel spacing($\Delta\lambda_{ch}$) is 3.2 nm and the adjacent wavelength channel crosstalk is about −13 dB. However, the performance of the AWG is seriously susceptible to phase errors. More compact channel spacing will cause more phase errors, which introduce larger crosstalk and insertion loss [13], [15]. There are some alternatives for WDM devices, such as cascaded Mach-Zehnder interferometers (MZIs) [16], [17], [18], bragg gratings [19], [20], as well as microring resonators (MRRs) [21], [22], [23]. Cascaded MZIs with low loss and low crosstalk are commonly applied to coarse wavelength division multiplexing (CWDM) [16], [24].

However, the footprints of the cascaded MZIs are pretty large when the wavelength-channel spacing is small. Bragg gratings have the same problem in footprints [25]. In contrast, MRR arrays can realize a low loss, low crosstalk WDM filter with a compact footprint. In [26], a 96-channel hybrid PDM-MDM-WDM (de)multiplexer was realized by monolithically integrating a 6-channel mode/polarization (de)multiplexer and 16-wavelength-channel microring resonators (MRRs) arrays. In [27], a 16-channel PDM-WDM (de)multiplexer was realized by using a

Manuscript received 4 February 2023; revised 20 March 2023; accepted 9 April 2023. Date of publication 12 April 2023; date of current version 26 April 2023. This work was supported in part by the National Key Research and Development Plan of China under Grant 2018YFB2200202, and in part by the National Science Foundation of China under Grant 61804148. *(Corresponding author: Huan Guan.)*

Hang Yu, Yuxiang Yin, Xingrui Huang, and Donghe Tu are with the State Key Laboratory on Integrated Optoelectronics, Institute of Semiconductors, Chinese Academy of Sciences, Beijing 100083, China, and also with the College of Materials Science and Opto-Electronic Technology, University of Chinese Academy of Sciences, Beijing 100083, China (e-mail: yuhang@semi.ac.cn; yinyuxiang@semi.ac.cn; xrhuang@semi.ac.cn; tudonghe@semi.ac.cn).

Zhiguo Yu, Huan Guan, and Zhiyong Li are with the State Key Laboratory on Integrated Optoelectronics, Institute of Semiconductors, Chinese Academy of Sciences, Beijing 100083, China (e-mail: zgyu@semi.ac.cn; yiyigh@semi.ac.cn; lizhy@semi.ac.cn).

Digital Object Identifier 10.1109/JPHOT.2023.3266393

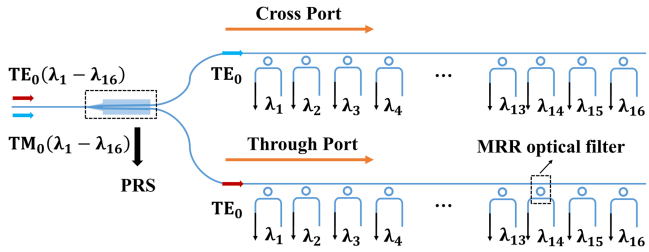

Fig. 1. The schematic configuration of the present hybrid PDM-WDM (de)multiplexer.

PRS and an 8-channel cascaded MRRs array. The wavelength-channel spacing is $\Delta\lambda_{ch} = 3.2$ nm and the polarization crosstalk is less than -20 dB. The capacity of data transmissions can be further increased by reducing the wavelength spacing. However, the high-order cascaded microrings structure is usually used in the case of wide wavelength spacing due to its wide 3-dB bandwidth. In addition, the resonance wavelengths of the MRRs are sensitive to the fabrication errors and environment temperature. It's challengeable to achieve the precise alignment to the resonance wavelengths. Therefore, thermal tuning is necessary for the resonance wavelength alignment of the MRRs array in dense wavelength division multiplexing (DWDM) systems.

In this article, we propose and experimentally demonstrate a silicon-based 32-channel hybrid PDM-WDM (de)multiplexer by combining a polarization rotator and splitter (PRS), and two 16-wavelength-channel MRRs arrays. The PRS consists of a bi-level adiabatic taper, a symmetric micro Y-branch and adiabatic couplers (ACs). The through and cross ports of the PRS are connected to the bus waveguide of the MRRs arrays. The wavelength-channel spacing in the present configuration is $\Delta\lambda_{ch} = 1.6$ nm, the crosstalk between the adjacent channels and non-adjacent channels are less than -20 dB and -25 dB respectively. For the hybrid (de)multiplexer, when TE_0 mode inputs, the insertion loss is 1.5 dB–3.8 dB. And the crosstalk between the through and cross port is less than -24 dB. When TM_0 mode inputs, the insertion loss is 1.9 dB–4.5 dB and the polarization crosstalk is less than -22 dB. In addition, we use thermal tuning to eliminate the influence of the fabrication errors and environment temperature on resonance wavelength.

II. Structure and Design

Fig. 1 shows the schematic of the proposed 32-channel PDM-WDM hybrid (de)multiplexer. The basic structure is realized by combing a PRS and two MRRs arrays, which realize a dual polarizations (de)multiplex and a 16-channel wavelength (de)multiplex, respectively.

For the polarization (de)multiplex, the PRS consists of a bi-level adiabatic taper, a symmetric Y-branch, and ACs. There are two main stages in the working process of PRS. The first stage is the rotation of polarization. TM_0 mode is converted into TE_1 mode by using a bi-level adiabatic taper due to mode hybridization mechanism. In the second stage, according to phase matching conditions, the incident is divided into equal parts by a symmetric Y-branch. Afterward, TE_1 mode is coupled to the cross port and converted to TE_0 mode, and the original TE_0 mode in the waveguide is coupled to through port. Fig. 2 shows the structural parameters of the PRS. In this way, the incident TE_0 mode and TM_0 mode are separated, and all converted to TE_0 mode.

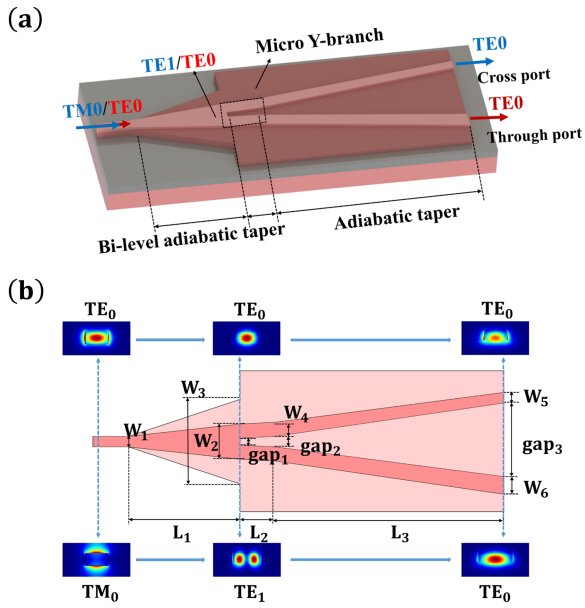

Fig. 2. (a) The three-dimensional view of the designed PRS consisting of a bi-level adiabatic taper, a symmetric Y-branch and ACs. (b) The structural parameters of the PRS.

Based on the mode hybridization mechanism, the bi-level adiabatic taper breaks the vertical symmetry, and thus forms a mode hybridization region. The width of the input strip waveguide is 0.4 μm, which is used for the injection of TE_0 mode and TM_0 mode. The height of the slab (h_1) is chosen as 70 nm to be compatible with the fabrication process. In order to satisfy the mode evolution condition, the width of the bi-level adiabatic taper needs to cover the mode hybridization region. Fig. 2(b) shows the mode profiles at different positions along the PRS. We define the initial width of the bi-level adiabatic taper $W_1 = 0.4$ μm to connect the input waveguide, and the end width of rib and slab are $W_2 = 1.18$ μm and $W_3 = 2.4$ μm to realize the mode conversion. When signal light transmitted from the bus waveguide injects into the bi-level adiabatic taper, TM_0 mode is converted to TE_1 mode and TE_0 mode remains the same polarization. To increase the mode conversion efficiency, the length of the bi-level adiabatic taper should be optimized. We used the EME solver of Lumerical to optimize the length of the taper and finally identified the length of the bi-level adiabatic taper (L_1) is 42 μm.

The Y-branch and ACs are employed to separate the TE_0 and TE_1 modes, and convert them to TE_0 mode in output ports. The Y-branch is a symmetrical structure, when TE_0 and TE_1 mode input, they are split into two equal parts and coupled into ACs. To ensure a high coupling efficiency of subsequent ACs, the divergence angle of the Y-branch should be very small. We set up a suitable $gap_1 = 0.18$ μm between the initial parts of the two waveguides to decrease the fabrication difficulty. In addition, we set a gradient region before the ACs ($L_2 = 8$ μm, $gap_2 =$

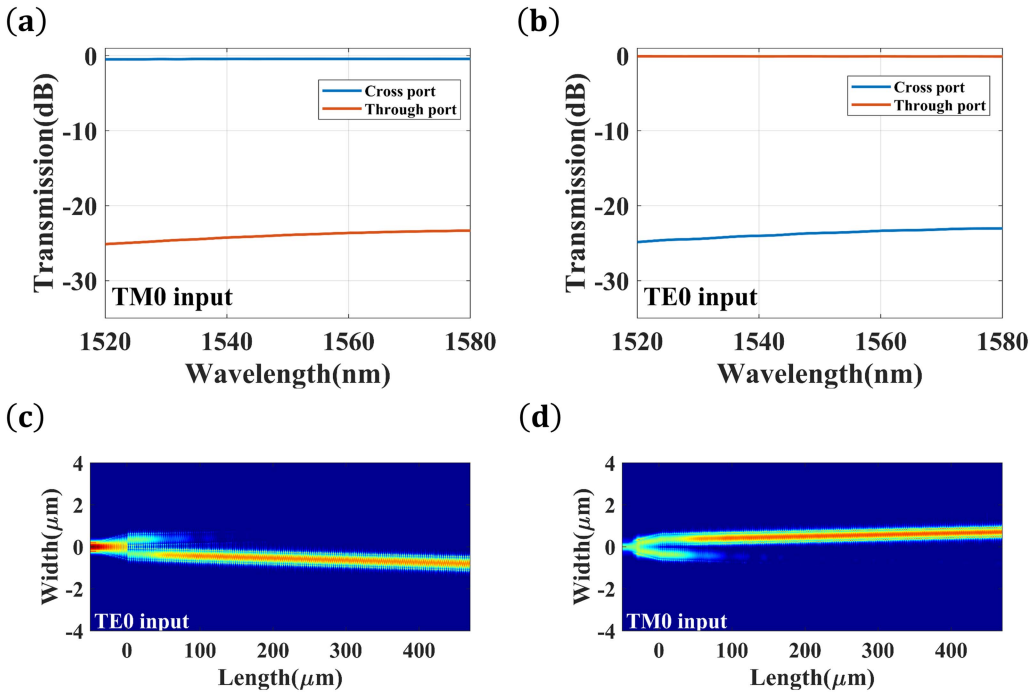

Fig. 3. (a) and (b) are the simulated spectral transmission at the through-port and cross-port when TE_0 mode and TM_0 mode are launched, respectively. (c) and (d) are the propagation field of the PRS when TE_0 mode and TM_0 mode are launched, respectively.

0.2 μm). In this way, the whole structure is within the fabrication tolerance. The two waveguides of ACs are adiabatically tapered from $W_4 = 0.5$ μm to $W_5 = 0.4$ μm and $W_6 = 0.6$ μm. According to the coupled mode theory, the input TE_1 mode will evolve to TE_0 mode in the narrow waveguide while the input TE_0 mode will evolve to TE_0 mode in the wide waveguide. To ensure the decoupling between the two output ports, the gap between the two waveguides is linearly varied and the terminal gap is chosen as $gap_3 = 1$ μm. To get low crosstalk, we optimize the length of the ACs and L_3 is 450 μm.

After the simulation of all unit parts, a complete PRS model is simulated. Fig. 3(a)–(d) shows the simulated transmission spectra and light propagation of the two output ports when TE_0 and TM_0 modes are input, respectively. In the wavelength range of 1520 nm–1580 nm, the PRS exhibits a good performance with the crosstalk between the adjacent ports less than -24 dB and -23 dB respectively. It also shows that it has a broad operating wavelength range. As a result, the designed PRS can support many wavelength-channels for WDM.

A compact MRRs array is used to realize the 16-channel WDM. The MRR array is designed based on strip waveguides. A low loss rib-to-strip converter is used in the output ports of the PRS. The width of the bus waveguide is $W_{bus} = 0.35$ μm, which supports TE_0 mode transmission well. To achieve a large FSR to cover all the multiplexed wavelength and meanwhile ensure a negligible bending loss, the microring radius need to be trade-off. According to the simulation results, the microring radius is set to about $R = 3$ μm and the microring waveguide width W_r is 0.5 μm. In order to align the wavelength spacing, the circumference difference between adjacent microrings is 32 nm, which is equivalent to the difference in radius of 5.093 nm. The corresponding FSR is 30.1 nm, which is enough to cover 16 channels when $\Delta\lambda_{ch} = 1.6$ nm. In addition, to achieve a high extinction ratio (ER), the gap between the microring and the bus waveguide is designed to be $gap_3 = 0.2$ μm, which approach critical coupling condition within the fabrication tolerance. The resonance wavelength of the MRR is seriously sensitive to fabrication deviation and environment temperature. To solve the problem, a TiN electrode with a resistance of 1000 ohms is used to align the resonance wavelength.

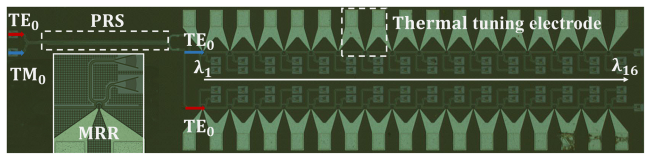

Fig. 4. The microscope image of the fabricated hybrid PDM-WDM (de)multiplexer.

III. Fabrication and Measurement

The proposed device was designed and fabricated on the SOI substrate with a 220-nm-thick top-silicon layer and a 2-μm-thick BOX layer. Fig. 4 shows the microscope picture of the fabricated hybrid PDM-WDM (de)multiplexer. Here the TE_0 mode and TM_0 mode grating couplers work not only for the highly efficient coupling but also suppress other polarizations. To ensure two modes can inject simultaneously, an extra TM_0 mode coupler was added.

The transmissions of the fabricated hybrid PDM-WDM (de)multiplexer were characterized by using a broadband source and an optical spectrum analyzer. The polarization of the injected light was selected by using a polarization controller. Fig. 5 shows the measured transmissions of the PRS when two polarizations

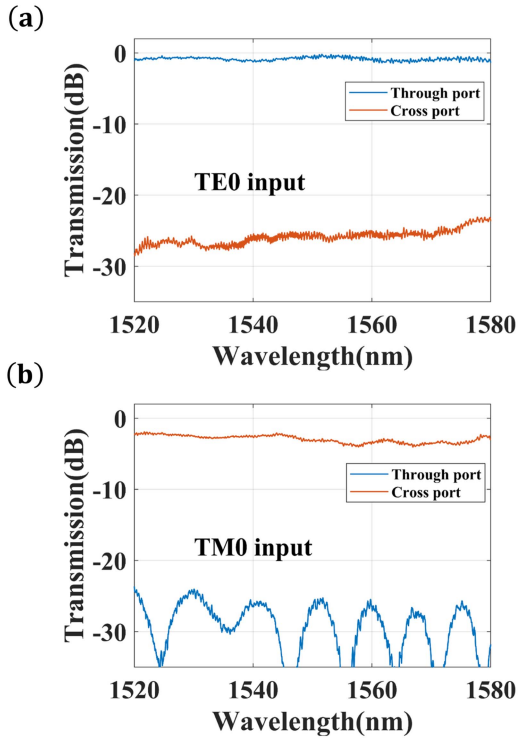

Fig. 5. The measured transmission spectra of the fabricated PRS under (a) TE_0 mode input and (b) TM_0 mode input.

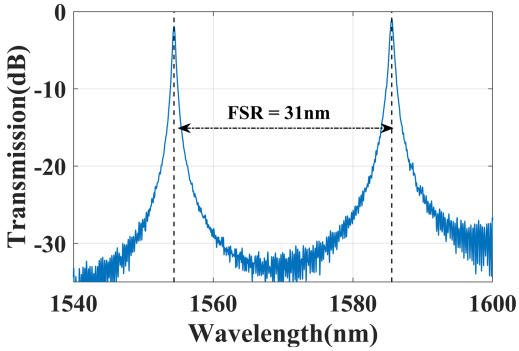

Fig. 6. Measured spectral response of an MRR.

are launched. The results have been calibrated by the response of the grating coupler and the TM_0 mode coupler. The total length of the PRS is 500 μm. When TE_0 mode is incident, the insertion loss is smaller than 1 dB at the through port, and the crosstalk between the through and cross ports is less than -24 dB from 1520 nm to 1580 nm. When TM_0 mode inputs, the crosstalk is less than -22 dB and the insertion loss is smaller than 3 dB. It can be seen that the PRS has a high polarization conversion efficiency, low crosstalk, and a broad bandwidth, which satisfies the requirements for PDM.

Fig. 6 shows the measured spectral response at the drop-port when light is launched from the input-port. The measured insertion loss at the resonant wavelength is less than 1.9 dB, and the 3 dB bandwidth is approximately 0.5 nm. The FSR is 31 nm which is sufficient to cover the sixteen wavelength-channels with $\Delta\lambda_{ch} = 1.6$ nm.

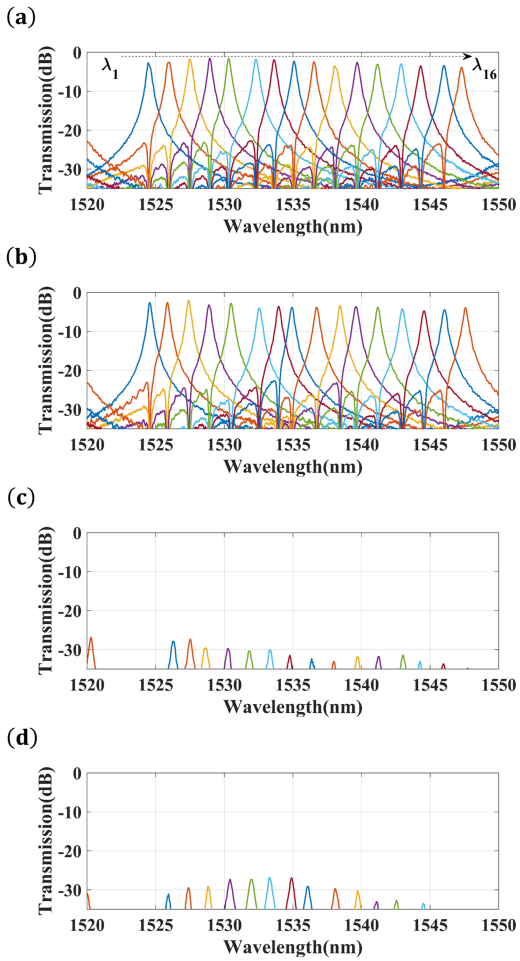

Fig. 7. Measured transmission spectral responses of the PDM-WDM hybrid multiplexer (a) TE_0 to through port, (b) TM_0 to cross port, (c) TE_0 to cross port (d) TM_0 to through port.

For the characterization of the fabricated hybrid WDM-PDM (de)multiplexer, light is incident from one of the input ports of the PRS, and selectively excited the corresponding polarization. After the polarization conversion by the PRS, the light is dropped by the corresponding MRRs array. Fig. 7 shows the measured spectral responses of the fabricated hybrid PDM-WDM (de)multiplexer in the wavelength range of 1520 nm–1550 nm, which covers an entire FSR. It can be seen that the insertion loss of the present hybrid PDM-WDM (de)multiplexer is 1.5 dB–3.8 dB when TE_0 mode inputs.

Here the insertion loss introduced by the PRS is less than 1 dB mentioned above. The crosstalk between the adjacent and non-adjacent wavelength channels are -20 dB and -25 dB respectively. In addition, the crosstalk between the through port and the cross port is less than -24 dB, which is almost in agreement with the experimental result of PRS. When TM_0 mode inputs, the insertion loss is 1.9 dB–4.5 dB, which is larger than TE_0 mode. The excess loss is mainly introduced by the PRS. It can be seen that there are fluctuations in insertion loss, which are caused by dispersion of coupling ratio, fabrication errors and measurement errors. The coupling ratio is wavelength dependent, which slightly varies with wavelength in a FSR.

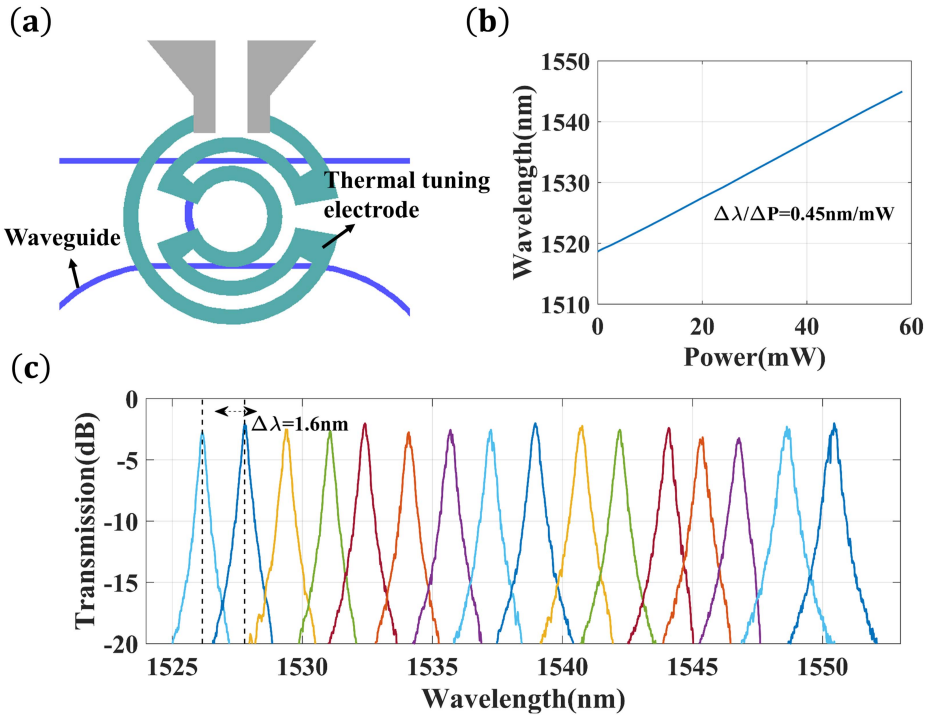

Fig. 8. (a) The schematic of the thermal tuning electrode. (b) The resonance wavelength as a function of the thermal power. (c) The transmission spectra after thermal tuning.

TABLE I
SUMMARY OF THE REPORTED PDM-WDM HYBRID (DE)MULTIPLEXER

Structure	N	$\Delta\lambda_{ch}$ (nm)	Loss (dB)	Wavelength crosstalk (dB)	3 dB-bandwidth (nm)	Polarization crosstalk (dB)	Ref.
PRS+AWG	18	3.2	7	< -13	/	< -10	[14]
2D Grating+AWG	32	1.6	15	< -21.5	1.16	/	[28]
PRS+MRRs	16	3.2	3	< -25	2	< -20	[27]
PRS+MRRs	**32**	**1.6**	**1.5 - 4.5**	**< -20**	**0.3-0.4**	**< -22**	**This work**

The fabrication errors mainly include two aspects, the deviation of the gap between bus waveguide and MRRs arrays and the deviations of different reference grating couplers. The variations of insertion loss are partly caused by measurement, including the alignment between the fiber and grating couplers, and the vibration of the test platform. The crosstalk between the adjacent and non-adjacent is similar with TE_0 mode, but the crosstalk between the through port and the cross port is less than -22 dB, slightly worse compared with TE_0 mode.

It can be noticed that there are some slight deviations for the channel spacing due to the fabrication deviation and environment temperature. Therefore, we used thermal tuning to calibrate the resonance wavelength. Based on the high thermal-optic coefficient, the resonance wavelength of MRRs arrays can be tuned precisely through the thermal tuning. The thermal tuning electrode of TiN is designed to maximize thermal tuning range and increase the maximum tolerated voltage to prevent breakdown. To achieve a large tuning range, a multi-wire structure electrode is designed to make the heat injection surface approximate a 1D heat flow in the direction perpendicular to the microring resonator, as shown in Fig. 8(a). To prevent breakdown, the length of the electrode was chosen to be 90 μm and the corresponding resistance was 1000 Ω. Fig. 8(b) shows the resonance wavelength as a function of the thermal power, which infers the tuning efficiency as 0.45 nm/mW. Fig. 8(c) shows the transmission spectra after thermal tuning, it can be seen that the channel spacing is approximately controlled at $\Delta\lambda_{ch} =$ 1.6 nm. Table I summarizes several recent works on PDM-WDM hybrid (de)multiplexer. Among all these (de)multiplexers, the demonstrated device has more channels which enhances the transmission capacity. The insertion loss, wavelength crosstalk, and polarization crosstalk all reach the mainstream level. And the advantage of this work is that the resonance wavelength can be aligned by thermal tuning, which corrects the deviation caused by fabrication errors and temperature vibrations. It's important for DWDM. Therefore, the proposed PDM-WDM

(de)multiplexer can meet the requirements of large capacity coherent optical transmitters.

IV. Conclusion

In summary, we have proposed and demonstrated a silicon-based hybrid PDM-WDM (de)multiplexer with 32 channels, including dual polarization channels and 16 wavelength channels. The present hybrid PDM-WDM (de)multiplexer was realized by monolithically integrating a PRS and two MRRs arrays. The through and cross ports of the PRS are connected to the bus waveguide of the MRRs arrays, the MRRs arrays are designed as a polarization selective device and work with resonances for TE_0 mode only. For the presented hybrid PDM-WDM (de)multiplexer, in the wavelength range from 1520 nm to 1550 nm, the 3 dB bandwidth is about 0.5 nm and the crosstalk of the adjacent channels and the non-adjacent channels are -20 dB and -25 dB, respectively. The resonance wavelength of the MRRs is controlled by thermal tuning with the tuning efficiency of 0.45 nm/mW, and the wavelength spacing is approximately 1.6 nm. When TE_0 mode inputs, the on-chip loss is 1.5 dB–3.8 dB and the crosstalk between the through and cross port is less than -24 dB. When TM_0 mode inputs, the insertion loss is 1.9 dB–4.5 dB and the polarization crosstalk is less than -22 dB. The experiment results show that the demonstrated high-performance PDM-WDM hybrid (de)multiplexer holds great potential for enhancing transmission capacity of the PIC.

Acknowledgment

The authors wish to thank H. Guan for her helpful suggestions.

References

[1] P. J. Winzer, D. T. Neilson, and A. R. Chraplyvy, "Fiber-optic transmission and networking: The previous 20 and the next 20 years," *Opt. Exp.*, vol. 26, no. 18, pp. 24190–24239, Sep. 2018.

[2] Y. Li, Y. Zhang, L. Zhang, and A. W. Poon, "Silicon and hybrid silicon photonic devices for intra-datacenter applications: State of the art and perspectives," *Photon. Res.*, vol. 3, no. 5, pp. B10–B27, Oct. 2015.

[3] P. G. Patki et al., "Recent progress on optical regeneration of wavelength-division-multiplexed data," *IEEE J. Sel. Topics Quantum Electron.*, vol. 27, no. 2, pp. 1–12, Mar./Apr. 2021.

[4] M. Singh, J. Malhotra, M. M. Rajan, V. Dhasarathan, and M. H. Aly, "Performance evaluation of 6.4 Tbps dual polarization quadrature phase shift keying Nyquist-WDM superchannel FSO transmission link: Impact of different weather conditions," *Alexandria Eng. J.*, vol. 59, no. 2, pp. 977–986, 2020.

[5] S. Pitris et al., "A 4×40 Gb/s O-band WDM silicon photonic transmitter based on micro-ring modulators," in *Proc. Opt. Fiber Commun. Conf. Exhibit.*, San Diego, CA, USA, 2019, pp. 1–3.

[6] P. Guo, W. Hou, L. Guo, Z. Ning, M. S. Obaidat, and W. Liu, "WDM-MDM silicon-based optical switching for data center networks," in *Proc. IEEE Int. Conf. Commun.*, 2019, pp. 1–6.

[7] D. Dai and J. E. Bowers, "Silicon-based on-chip multiplexing technologies and devices for Peta-bit optical interconnects," *Nanophotonics*, vol. 3, no. 4/5, pp. 283–311, 2014, doi: 10.1515/nanoph-2013-0021.

[8] Y. Tan, H. Wu, S. Wang, C. Li, and D. Dai, "Silicon-based hybrid demultiplexer for wavelength- and mode-division multiplexing," *Opt. Lett.*, vol. 43, no. 9, pp. 1962–1965, May 2018.

[9] O. M. Nawwar, H. M. H. Shalaby, and R. K. Pokharel, "Photonic crystal-based compact hybrid WDM/MDM (De)multiplexer for SOI platforms," *Opt. Lett.*, vol. 43, no. 17, pp. 4176–4179, Sep. 2018.

[10] P. Dong, "Silicon photonic integrated circuits for wavelength-division multiplexing applications," *IEEE J. Sel. Topics Quantum Electron.*, vol. 22, no. 6, pp. 370–378, Nov./Dec. 2016.

[11] M. Ye, Y. Yu, G. Chen, Y. Luo, and X. Zhang, "On-chip WDM mode-division multiplexing interconnection with optional demodulation function," *Opt. Exp.*, vol. 23, no. 25, pp. 32130–32138, Dec. 2015.

[12] T. Mulugeta and M. Rasras, "Silicon hybrid (De)multiplexer enabling simultaneous mode and wavelength-division multiplexing," *Opt. Exp.*, vol. 23, no. 2, pp. 943–949, Jan. 2015.

[13] J. Wang, S. Chen, and D. Dai, "Silicon hybrid demultiplexer with 64 channels for wavelength/mode-division multiplexed on-chip optical interconnects," *Opt. Lett.*, vol. 39, no. 24, pp. 6993–6996, Dec. 2014.

[14] S. Chen, Y. Shi, S. He, and D. Dai, "Compact monolithically-integrated hybrid (de)multiplexer based on silicon-on-insulator nanowires for PDM-WDM systems," *Opt. Exp.*, vol. 23, no. 10, pp. 12840–12849, May 2015.

[15] J. Brouckaert, W. Bogaerts, P. Dumon, D. V. Thourhout, and R. Baets, "Planar concave grating demultiplexer fabricated on a nanophotonic silicon-on-insulator platform," *J. Lightw. Technol.*, vol. 25, no. 5, pp. 1269–1275, May 2007.

[16] T.-H. Yen and Y.-J. Hung, "Fabrication-tolerant CWDM (de)multiplexer based on cascaded Mach–Zehnder interferometers on silicon-on-insulator," *J. Lightw. Technol.*, vol. 39, no. 1, pp. 146–153, Jan. 2021.

[17] Q. Yi et al., "Silicon photonic flat-top WDM (de)multiplexer based on cascaded Mach-Zehnder interferometers for the 2m wavelength band," *Opt. Exp.*, vol. 30, no. 15, pp. 28232–28241, Jul. 2022.

[18] Z. Zhao et al., "Eight-channel LAN WDM (de)multiplexer based on cascaded Mach–Zehnder interferometer on SOI for 400GbE," *Photonics*, vol. 9, no. 4, 2022, Art. no. 252. [Online]. Available: https://www.mdpi.com/2304-6732/9/4/252

[19] D. Mu et al., "A four-channel DWDM tunable add/drop demultiplexer based on silicon waveguide Bragg gratings," *IEEE Photon. J.*, vol. 11, no. 1, pp. 1–8, Feb. 2019.

[20] Z. Huang and Y. Wang, "Four-wavelength III-V/SOI heterogeneous integrated laser based on sampled Bragg grating for CWDM," *IEEE Photon. J.*, vol. 5, no. 5, Oct. 2013, Art. no. 1501906.

[21] Y.-D. Yang, Y. Li, Y.-Z. Huang, and A. W. Poon, "Silicon nitride three-mode division multiplexing and wavelength-division multiplexing using asymmetrical directional couplers and microring resonators," *Opt. Exp.*, vol. 22, no. 18, pp. 22172–22183, Sep. 2014.

[22] A. Bagheri, F. Nazari, and M. K. Moravvej-Farshi, "Tunable optical demultiplexer for dense wavelength division multiplexing systems using graphene–silicon microring resonators," *J. Electron. Mater.*, vol. 49, no. 12, pp. 7410–7419, 2020.

[23] X. Guan, W. Shi, and L. A. Rusch, "Ultra-dense wavelength-division multiplexing with microring modulator," *J. Lightw. Technol.*, vol. 39, no. 13, pp. 4300–4306, Jul. 2021.

[24] H. Xu, D. Dai, and Y. Shi, "Low-crosstalk and fabrication-tolerant four-channel CWDM filter based on dispersion-engineered Mach-Zehnder interferometers," *Opt. Exp.*, vol. 29, no. 13, pp. 20617–20631, Jun. 2021.

[25] J. Jiang et al., "Silicon lateral-apodized add-drop filter for on-chip optical interconnection," *Appl. Opt.*, vol. 56, no. 30, pp. 8425–8429, Oct. 2017.

[26] W. Zhao et al., "96-channel on-chip reconfigurable optical add-drop multiplexer for multidimensional multiplexing systems," *Nanophotonics*, vol. 11, no. 18, pp. 4299–4313, 2022, doi: 10.1515/nanoph-2022-0319.

[27] Y. Tan, H. Wu, and D. Dai, "Silicon-based hybrid (de)multiplexer for wavelength-/polarization-division-multiplexing," *J. Lightw. Technol.*, vol. 36, no. 11, pp. 2051–2058, Jun. 2018.

[28] S. Pathak, M. Vanslembrouck, P. Dumon, D. V. Thourhout, and W. Bogaerts, "Compact SOI-based polarization diversity wavelength demultiplexer circuit using two symmetric AWGs," *Opt. Exp.*, vol. 20, no. 26, pp. B493–B500, Dec. 2012.